Fourier-constrained blind restoration of imagery obtained in poor imaging conditions

Douglas A. Hope, Stuart M. Jefferies[a,b], Cindy Giebink
Institute for Astronomy, Univ.of Hawaii, Advanced Technology Research Center, Pukalani, HI
[a]Steward Observatory, Univ. of Arizona, 933 N Cherry Ave., Rm. N204, Tucson, AZ 85721
[b]Physics and Astronomy Department, Univ. of New Mexico, 800 Yale, Albuquerque, NM 87131

ABSTRACT

Random fluctuations in the index of refraction, caused by differential heating and cooling of the atmosphere, can severely limit the quality of ground-based observations of space objects. Techniques such as adaptive optics can help compensate for the deleterious effects that turbulence has on the images by deforming the telescope mirror and thus correcting the wave-front. However, when imaging through strong turbulence such techniques may not adequately correct the wave-front. In such cases blind restoration techniques – which estimate both the atmospheric turbulence characterized by the atmospheric point-spread-function and the object that is being observed - must be used. We demonstrate high quality blind restorations of object scenes, obtained when observing through strong turbulence, by using a sequence of images obtained simultaneously at different wavelengths and prior information on the distribution of the sources of regions of low spectral power in the data.

Keywords: Inverse problems, Image restoration

1. INTRODUCTION

Blind restoration is an important post-processing technique for restoring imagery when the point spread function (PSF) for the imaging system is either not known or is poorly known. Perhaps one of the most widely used blind restoration techniques is multi-frame blind deconvolution (MFBD)[1,2] This technique is used for sequences of images of a target obtained over time scales such that the target can be considered stationary but the PSFs are changing. This situation is common for observations of objects through the Earth's atmosphere where fluctuations in the air temperature at the interface between different layers of air, give rise to random fluctuations in the refractive index of the air. These fluctuations produce aberrations in any wave front propagating through the air (hence yielding a changing PSF). Though adaptive optics (AO) can compensate for these randomly induced aberrations, this compensation is never complete especially in regimes of strong turbulence where post-processing is often applied to AO data.

The blind restoration problem is typically both ill-conditioned (due to noise in the measurements) and ill-posed (i.e. it does not have a unique solution[3]). However, one can find physically meaningful solutions by using prior information about the object being viewed (e.g., spatial extent, positivity, real-plane zeros[4]) and knowledge about the underlying physics of the imaging process. In general, the fidelity and resolution of the restoration is directly related to the amount and quality of prior information used to constrain the restoration. Here we investigate a new information prior that is based on the fact that not all spatial frequencies in the data carry the same amount of information. We combine this new constraint with current wavelength diversity[5] image restoration methods to obtain high fidelity image restorations using data obtained when the target is observed through strong turbulence.

We restrict our studies to imagery that is obtained under isoplanatic conditions, that is, the PSFs are spatially invariant. This allows us to describe the observed imagery $g_k(\mathbf{x})$ in terms of a convolution of the target object $f(\mathbf{x})$ and PSF $h(\mathbf{x})$ plus additive noise $n_k(\mathbf{x})$. That is,

$$g_k(x) = \sum_{x'} f(x') h_k(x - x') + n_k(x), \tag{1}$$

where the subscript *k* denotes a time index. Equivalently, the observed Fourier spectra are represented by

$$G_k(u) = F(u)H_k(u) + N_k(u). \quad (2)$$

Isoplanatic conditions will apply when the main source of atmospheric turbulence is close to the telescope aperture.

2. SPECTRAL HOLES

Spatial frequencies in the data that have low Fourier power carry little or no information. We refer to such frequencies as *spectral holes*. Equation (2) shows that, in spectral regions where the signal-to-noise ratio is greater than unity, spectral holes in the data are a direct result of holes in the spectra of the object and PSF. In general, the source of an individual hole is unknown. However, when imaging a stationary object through the turbulent atmosphere, the spectral holes in the data associated with the PSF will change from frame to frame while the holes that are part of the object spectrum will remain fixed. This allows us to identify the source of each hole and thus determine the distribution of the spectral holes between the PSF and object.

Interestingly, the Fourier spectra of man-made objects such as spacecrafts and satellites appear to have a large fraction of the spectrum that can be omitted before any significant visual impact is noticed (see Fig. 1)

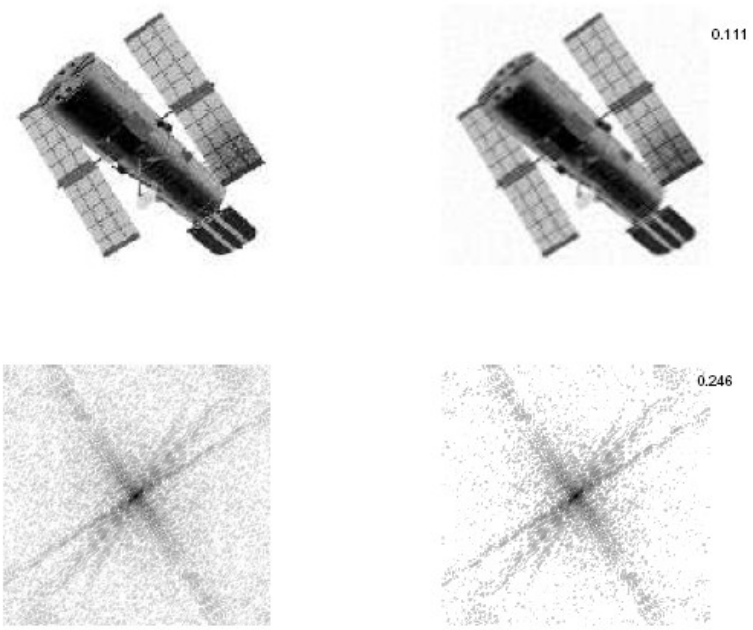

Figure 1 Left column: Model of the Hubble Space Telescope [top] and its full Fourier spectrum [bottom]. Right column: Fourier-constrained object where the threshold for identifying spectral holes is 10^{-5} of the peak object power. The number in the upper right hand corner of the top panel denotes the relative (r.m.s.) error between the truth and the Fourier-constrained target scene, that is the scene after spectral holes are excluded from the spectrum, while the number in the bottom panel denotes the fractional amount of the Fourier spectrum that is present in the constrained scene.

Knowing the locations of these regions of low power (spectral holes) should therefore provide a strong prior constraint on the object during the image restoration process. Similarly, knowledge of the spectral-hole structure for the PSF should aid in the recovery of the PSF. The leverage gained from using this prior information on the PSF, however, will depend on the strength of the turbulence and the extent of the power spectrum of the object. The former is because the number of PSF spectral holes increases as the turbulence strength increases (see Figs. 2 & 3). The latter is a consequence of how we identify PSF spectral holes (see below), basically they can only be identified in regions where the object spectrum has signal.

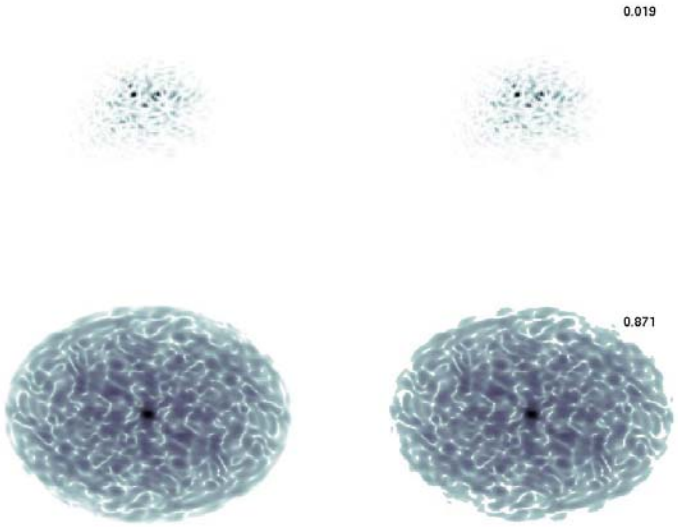

Figure 2 Left column: PSF for D/r0 = 15 [top] and its Fourier power spectrum [bottom] Right column: Fourier constrained PSF [top] where spectral frequencies with power below 10^{-5} have been identified as spectral holes. The number in the upper right corner is the relative error between the truth and constrained PSF while the number in the lower right is the fraction of Fourier frequencies within the PSF diffraction band-limit that remain after applying the threshold.

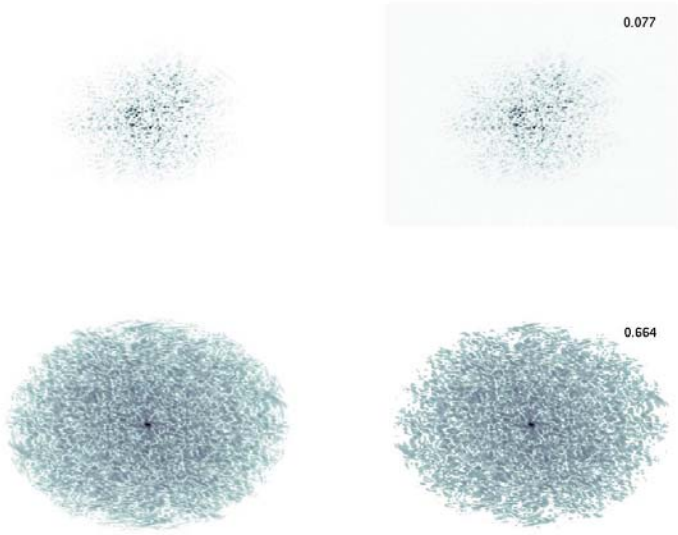

Figure 3 Left column: PSF for D/r0 = 80 [top] and its Fourier power spectrum [bottom] Right column: Fourier constrained PSF [top] where spectral frequencies with power below 10^{-5} have been identified as spectral holes. The number in the upper right corner is the relative error between the truth and constrained PSF while the number in the lower right is the fraction of Fourier frequencies within the PSF diffraction band-limit that remain after applying the threshold.

Our method for identifying the sources of the observed spectral holes relies on the fact that for a sufficiently large data ensemble, the average power spectrum of the PSFs is expected to be nonzero out to the diffraction-limit of the observations[6]. With this assumption we compute the ensemble SNR,

$$SNR(u) = \sqrt{N}\,\frac{\left\langle |G(u)|^2 - |N(u)|^2 \right\rangle}{\sigma_G} \tag{3}$$

where N denotes the number of frames and σ_G denotes the error due to the random nature of atmospheric turbulence. The noise bias $|N(u)|^2$ is estimated from spatial frequencies beyond the diffraction cut-off frequency. We then define a spectral frequency as being an object spectral hole if the SNR at that frequency is below some user set threshold T_F. One basis for setting the value of, T_F, is that it should equal some minimum value of SNR.

Once the object holes are known the PSF spectral holes can be computed for each frame using the individual frame SNR,

$$SNR_k(u) = \frac{\left\langle |G_k(u)|^2 \right\rangle}{\sigma_N} \tag{4}$$

where σ_N denotes the standard deviation of the additive noise-process. Spatial frequencies in frames where the $SNR_k(u)$ is below a threshold T_H are then associated with spectral holes of the PSF. It is obvious that we can only identify PSF spectral holes where there is signal in the spectrum of the object. This means that we usually only have knowledge of a subset of the PSF spectral holes. Finally, we note that spectral holes can only be clearly identified in data when the target signal is completely captured by the imaging array. Any truncation of the signal by the detector array will lead to artificial zeros in the Fourier spectra of the observed data.

3. IMAGING AT MULTIPLE WAVELENGTHS

Imaging a target scene simultaneously at multiple wavelengths enables one to obtain information about materials on the target and to acquire additional constraints on turbulence induced wave perturbations in the telescope pupil. The strength of these perturbations is related to the Fried parameter r_0 parameter which scales as[7]

$$r_0^I = r_0^V \left(\frac{\lambda_I}{\lambda_V} \right)^{6/5} \tag{5}$$

where λ_V and λ_I denote the observation wavelengths in the visible and infrared respectively, while r_0^V and r_0^I are Fried parameter values at these wavelengths. For multi-wavelength observations when the exposure time is less than or equal to the atmospheric coherence time, i.e. $\tau_e \le \tau_{atm}$, the wave-front phase at the j^{th} wavelength can be expressed as,

$$\theta_j(u) = \frac{2\pi}{\lambda_j} W(u) \tag{6}$$

where W(u) denotes an optical path difference that is common for all channels. The phase when expressed in terms of the common OPD, which can be represented using a convenient basis such as Zernike polynomials, can easily be scaled to another wavelength. In MFBD one can use this fact to estimate the phases at the longer wavelength, where the turbulence is less severe and then scale these phases to use as an initial seed when restoring the imagery at the shorter wavelength where the turbulence is more severe.

4. MFBD ALGORITHM USING SPECTRAL HOLES AND COMMON OPD

We model the object and PSF intensity distributions at the j^{th} wavelength using the model,[8]

$$a_j(x) = \phi_j(x)\phi_j(x)^* \tag{7}$$

which enforces our prior knowledge that both functions must be real and positive. The variables of this model can be defined in either the image domain or in the Fourier domain. In the latter case we use the re-parameterization

$$\begin{aligned}\phi_j(x) &= F^{-1}\left\{\Phi_j(u)M_j(u)\right\} \\ &= F^{-1}\left\{M_j(u)P_j(u)e^{i\theta_j(u)}\right\}\end{aligned} \tag{8}$$

where F^{-1} denotes the inverse Fourier Transform and $M_j(u)$ is a real-valued binary mask that is defined over the central N/2 x N/2 region of the pixel array used to model $\Phi_j(u)$. Here we choose the image domain for modeling the object, (i.e. $\phi(x)$ are the variables) and the Fourier domain for modeling the PSFs (i.e. $P(u)$ and $\theta(u)$ are the variables. The choice was based on the fact that the latter version of the model directly incorporates the physics of the imaging system - $P(u)$ and $\theta(u)$ represent the wave-front amplitudes (assumed unitary for isoplanatic imaging), the phase expressed in terms of OPD via Eq. (6) , respectively, and $M(u)$ incorporates information on the pupil of the telescope – while the former version allows prior knowledge of the morphology of the object to be straightforwardly incorporated into the deconvolution problem. In the case of long exposure AO imaging (when $\tau_e >> \tau_{atm}$ where τ_e and τ_{atm} denote the exposure time and the atmospheric coherence time respectively) or when scintillation (variations in the wave-front amplitudes) are present, Eq. (8) is an appropriate model for the PSF. In this work we focus on short exposure AO imagery (when $\tau_e \le \tau_{atm}$) and ignore the effects of scintillation and only estimate variations in the wave-front phases.

The variables in the image model are determined using a conjugate gradient algorithm to minimize the cost function

$$\varepsilon = \sum_l \alpha_l \varepsilon_l \tag{9}$$

where the individual components ε_l represent the enforcement of different prior information. For this work we have three terms, $(l = 0...2)$, ε_0 measures the error between the data model and the actual data, while ε_1 and ε_2 penalize energy at spatial frequencies defined to be spectral holes in the object and PSF respectively. The ε_0 component is given by

$$\varepsilon_0 = \sum_k \sum_x r_k^2(x) \tag{10}$$

where,

$$r_k(x) = d_k(x)\frac{\hat{g}_k(x) - g_k(x)}{\sqrt{\hat{g}_k(x) + \sigma_N^2}}. \tag{11}$$

Here $d_k(x)$ is a binary data mask with zeros at locations of bad pixels or pixels with a low image domain SNR and $g_k(x)$ represents the observed data at different times (k). In the denominator, $\hat{g}_k(x)$ and σ_N, represent the Gaussian and Poisson components of the noise variance respectively[9]. The remaining ε_l components are given by

$$\varepsilon_l = \sum_k \sum_u M_k^{hole}(u) \left| A_k(u) \right|^2 \tag{12}$$

where $A_k(u)$ is the Fourier transform of $a(x)$ and M_k^{hole} (u) is computed via Eq. (3) or (4) depending on the type of spectral hole.

We note that, ideally, the ε_l should mimic a probability density function so that $\alpha_l = 1$ for all l. However, it is not always practical to achieve this requirement and values of α_l need to be determined that will provide the best solution. Here we define $\alpha_0 = 1$ and choose the values of $\alpha_{l \neq 0}$ such that the derivatives $\frac{\partial \varepsilon_l}{\partial \theta_k(u)}$ are all similar in magnitude at the beginning of the iteration. We have found that this results in values for α_l that are close to optimal.

5. RESULTS

We present MFBD restorations using simulated short exposure AO-imagery ($\tau_e \leq \tau_{atm}$ where τ_e and τ_{atm} denote the exposure time and the atmospheric coherence time respectively) obtained in strong atmospheric turbulence characterized by $D/r_0 = 80$ where D denotes the diameter of the telescope pupil. A "lucky shot" data frame is shown in Fig 4. When running MFBD algorithms on data obtained in this regime of turbulence, the algorithm will typically stagnate due to local minima in the parameter space. An example of one such minimum is shown on the left in Fig. 5 where a restoration was obtained using a pixel basis for representing the object and the wave-front phases. Avoiding entrapment into such minima require two important elements: 1) a good initial start that should be as close to the actual solution as possible and 2) the use of additional constraints such as knowledge about the location of object and PSF spectral holes.

Our strategy for overcoming the stagnation problem in strong turbulence was to image the object simultaneously at infrared (1.6 μm) and visible (0.425 μm) wavelengths. An MFBD restoration was performed on the infrared data (where the turbulence is less severe) using PSF spectral holes to obtain a point-by-point estimate of the wave-front phase. These phases were decomposed using a Zernike basis and the coefficients for each Zernike mode were scaled appropriately to visible wavelengths. Though these phases only contain information on low order spatial frequencies in the PSF, their knowledge is an excellent initial guess for starting the minimization. Furthermore, we enforce additional constraints on the Fourier frequencies in the object and PSF via spectral holes. By using both the common OPD and spectral holes we satisfy both requirements outlined above. Shown on the left in Fig 5 the restoration that was obtained when using a poor initial start (zero wave-front phases), while on the right is the restoration when we supply a good initial start, obtained from the infrared data, and constraints on the object and Fourier spectrum expressed via the spectral holes. This ability to extract meaningful information from data obtained through strong turbulence conditions means that we can dramatically extend the range of conditions for successfully identification and monitoring of spaced-based targets.

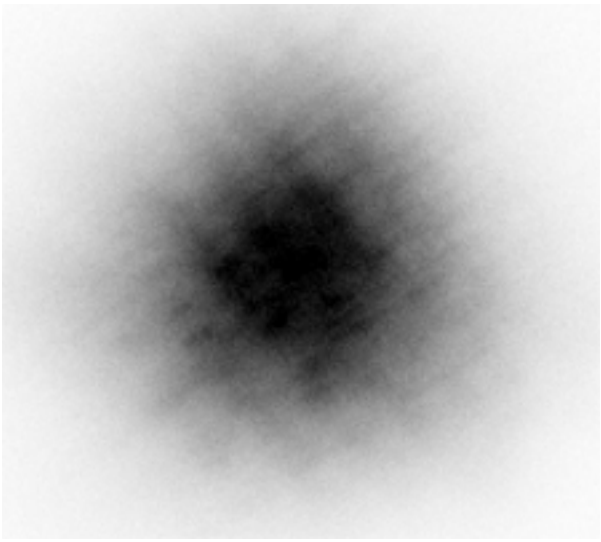

Figure 4 Shown is a "lucky shot" data frame for $D/r_0 = 80$

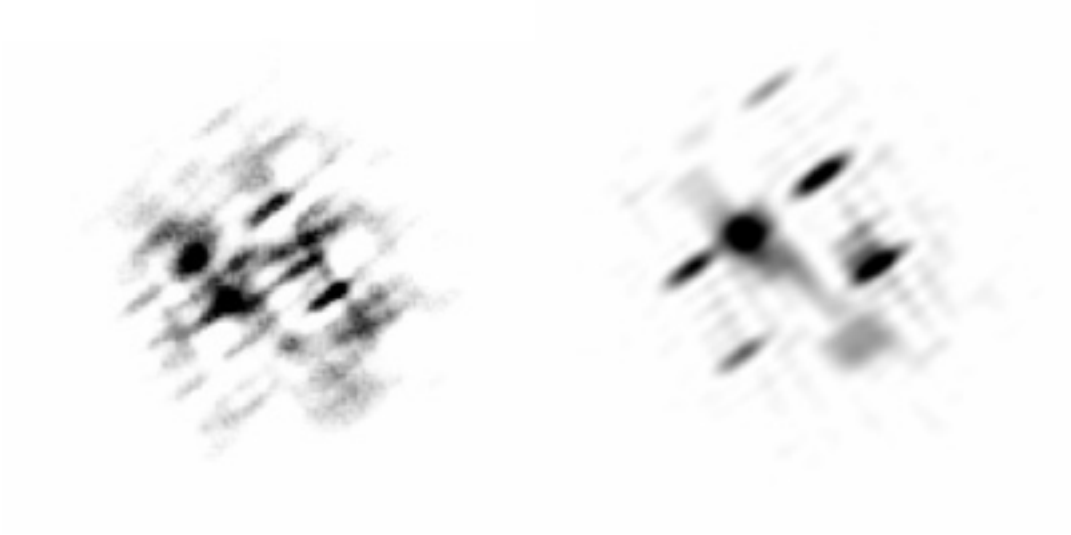

Figure 5 Left: Image restoration using a pixel basis for the object and the wave-front phase for $D/r_0 = 80$ and no spectral hole information. Right: Image restoration using same approach but use of spectral holes and common OPD for $D/r_0 = 80$. The truth object is shown in Fig 1.

ACKNOWLEDGEMENTS

This work was performed under awards F9550-06-1-0179 and F49620-02-1-0107 from the Air Force Office of Scientific Research. The restorations were performed on computers at the Maui High Performance Computing Center (award F29601-01-D-0083) and the Western Australia Supercomputer Center.

REFERENCES

[1] T. J. Schulz, "Multi-frame blind deconvolution of astronomical images," J. Opt. Soc. Am. A, **10** 1064-1073 (1993)

[2] S. M. Jefferies and J. C. Christou, "Restoration of Astronomical Images by Iterative Blind Deconvolution," Astrophys. J., **415**, 862 (1993)

[3] A. N. Tikhonov.and V. Y. Arsenin, Methods for Solving Ill-posed problems, Nauka, Moscow. (1979)

[4] P. Chen, M. A. Fiddy, C.W. Liao and A. Pommet, "Blind deconvolution and phase retrieval from point zeros," J. Opt. Soc. Am. A. **15**, 7 (1996)

[5] H. R. Ingleby and D. R. McGaughey, "Real data results with wavelength-diverse blind deconvolution," Opt. Letters **30**, 5, 489-490 (2005).

[6] A. Labeyrie, "Attainment of Diffraction Limited Resolution in Large Telescopes by Fourier analyzing Speckle Patters in Star Images," Astron. Astrophys. **6**, 85 (1970)

[7] F. Roddier, "Imaging through the atmosphere," Adaptive Optics in Astronomy, F.Roddier; editor, 9-24, Cambridge University Press London 1999.

[8] N. Miura, "Blind deconvolution of band limited images," Optics Letters, **28**, 2312-2314 (2003)

[9] S. M. Jefferies, M. Lloyd-Hart, E. K. Hege, and J. Georges, "Sensing wave-front amplitude and phase with phase diversity," Applied Optics **41**, 11 2095-2102 (2002)